atmosphere

MDPI

Article

Assessing the Impact of Natural Conditions/Socioeconomic Indicators on the Urban Thermal Environment Based on Geographic Big Data

Xiaolong Lu [1,2,*], Haihui Wang [1,2], Huanliang Chen [1,2] and Shuai Gao [1,2]

[1] 801 Institute of Hydrogeology and Engineering Geology, Shandong Provincial Bureau of Geology & Mineral Resources, Jinan 250000, China
[2] Shandong Engineering Research Center for Environmental Protection and Remediation on Groundwater, Jinan 250000, China
* Correspondence: xlonglu@163.com

Abstract: Understanding correctly the factors influencing the urban thermal environment is a prerequisite and basis for formulating heat-island-effect mitigation policies and studying urban ecological issues. The rapid urbanization process has led to the gradual replacement of natural landscapes by products of socioeconomic activities, and although previous studies have shown that natural conditions and socioeconomic intensity can significantly influence land surface temperature (LST), few studies have explored the combined effects of both on LST, especially at a fine scale. Therefore, this study investigated the relationship between natural conditions/socioeconomic and summer daytime LST based on big data and a random forest (RF) algorithm using the city of Jinan as the study area. The results showed that the spatial pattern of LST, natural condition characteristics of the city, and socioeconomic characteristics are consistent in spatial pattern and have significant correlation. In the RF model, the fitted R^2 of the regression model considering two influencing factors reaches 0.86, which is significantly higher than that of the regression model considering only one influencing factor. In the optimal regression model, topographic factors in natural conditions and socioeconomic factors in buildings and roads are very important factors influencing the urban thermal environment. Based on the results, strategies and measures for developing and managing measures related to the thermal environment are discussed in depth. The results can be used as a reference for mitigating urban heat islands in the study area or other cities with similar characteristics.

Keywords: land surface temperature; random forest; geographic big data

Citation: Lu, X.; Wang, H.; Chen, H.; Gao, S. Assessing the Impact of Natural Conditions/Socioeconomic Indicators on the Urban Thermal Environment Based on Geographic Big Data. *Atmosphere* **2022**, *13*, 1942. https://doi.org/10.3390/atmos13121942

Academic Editors: Geng-Ming Jiang and Bo-Hui Tang

Received: 22 October 2022
Accepted: 17 November 2022
Published: 22 November 2022

1. Introduction

The urban heat island effect is a phenomenon in which the temperature of a city's downtown area is significantly higher than that of its suburbs [1]. With accelerated urbanization and continuous expansion, the urban heat environment issue is receiving increasing attention [2]. In recent decades, global warming has become a major threat to the sustainable development of human society, and relevant assessment reports indicate that global temperature will increase by 0.2–0.5 °C per decade within this century [3]. In this context, urban thermal environment monitoring has become a research hotspot in ecology, atmospheric science, and other disciplines [4]. Information quantifying the driving forces of temperature change within cities is critical to improving the urban thermal environment [5] in mid- and low-latitude regions, where significantly high temperatures can have significant adverse effects on urban ecosystems and public health [6,7]. Therefore, accurate analysis of the spatial pattern of the urban thermal environment and its influencing factors becomes critical to address this issue, and the results can provide insights to urban planners and designers [8], such as how to mitigate surface UHI (SUHI) effects during the summer daytime through sound landscape design and urban management.

The traditional method of monitoring the urban thermal environment relies on ground-based monitoring stations [9], but due to the specificity of the monitoring stations, it is practically impossible to provide values over large areas. With the continuous maturation of Earth observation technology and the rapid development of thermal infrared remote sensing, LST is gradually becoming a key parameter in physical processes on land surfaces from a local to a global scale [10,11]. The importance of LST is increasingly recognized, and it is used in a wide range of applications. Different satellite sensors, such as MODIS and Landsat, are widely used for LST retrieval. However, there are still some limitations in using LST inversion results from thermal sensors, such as the trade-off between spatial and temporal resolution of the images [12], where too high a spatial resolution often implies a long revisit period of the images, which makes it a topic of interest for future research. However, in general, inversion of LST employing remote sensing has become a widely used method, and provides the best data source for studying the urban thermal environment on a large scale [13].

With the application of remote sensing technology, many studies have focused on the analysis of the influencing factors of urban LST [14], and there is sufficient evidence that the urban thermal environment is an urban climate phenomenon that is influenced not only by overall climate change but also by the internal factors of the city itself, which is a collaborative effect of internal and external factors [15,16]. In general, the factors influencing the urban thermal environment include human activities in the urbanization process and the natural surface conditions themselves [17]. Specifically, human production and living activities generate a large amount of anthropogenic heat release, such as industrial production activities, motor vehicle exhaust emissions, and winter heating in cities, which will emit heat into the near-Earth layer of cities and have a significant impact on the urban LST [18,19]. Numerous researchers have achieved a series of results in analyzing the thermal effects of human activities, such as Giorgio et al., who confirmed the prevalence of the urban heat island phenomenon in industrialized areas by analyzing the thermal environment of industrial areas [20]. Some researchers have explored the driving mechanism of socioeconomic factors in the urban thermal environment and revealed the mechanism of human activities in the urban thermal environment [21,22]. Others have studied the synergistic relationship between human activities and the urban heat island effect and reached consistent conclusions that high-intensity human activities can deteriorate the urban thermal environment [23]. At the same time, there is evidence that city size and urban heat islands tend to show a positive correlation [24], which reflects that changes in natural conditions due to urbanization are also one of the main factors in the deterioration of the urban thermal environment [25]. For example, some researchers have analyzed the correlation between LST and topographic elements [26], and Chun, Bumseok et al. [27] confirmed through statistical analysis of building morphology and the urban thermal environment that high-density buildings exacerbate the heat island effect, and some studies have confirmed that hard impermeable surfaces, such as pavements, change the urban subsurface structure and consequent changes in urban morphology and development intensity of various types of land in cities. Both qualitative and quantitative analyses show that changes in natural conditions/socioeconomic characteristics respond to the heat island effect, which poses new requirements for an integrated analysis of the effects of both on the thermal environment. However, accurate quantification of both characteristics requires high data requirements, especially the identification of socioeconomic characteristics, which demands data at finer scales and enriched with more attributes.

In recent years, with the widespread use of online electronic maps, POIs (points of interest), online data open platforms, and other software, new data support for geographic research has been provided [28,29], generating a large amount of multisource geographic data with location information, which contain rich information on urban characteristics, such as the location and time of urban elements [30]. Compared with remote sensing images, multisource geographic data have the characteristics of high presentability, fast dissemination, and low acquisition cost, which can provide new reference information

for various fields of urban research (such as feature measurement, classification, change detection, etc.) and provide a new data source for relevant research in the field of geography [31]. The processing and application of multisource geographic data have gradually received wide attention in recent years, and many researchers have already tried to apply multisource geographic data to urban research, such as applying it to perceive the spatial differentiation of cities [31], detection of urban hotspot areas [32], research of urban spatial structure [33], land use classification [34], etc., which fully proves that multisource geographic data can portray social, economic, humanistic and other nonnatural elements.

Based on the above background, there is a lack of reported research on natural conditions/socioeconomic indicators and quantitative models of the thermal environment, mainly because of the complex potential nonlinear relationships between LST and indicator components [35], which makes it a serious technical challenge to accurately assess the urban thermal environment situation. Therefore, this study introduces multisource data to comprehensively assess the impact of natural conditions/socioeconomic indicators on the urban thermal environment, using the central urban area of Jinan as the study area. Specifically, this study proposes an analytical framework of natural conditions/socioeconomic measures and their thermal environment impacts based on multisource geographic data, further refines the measurement criteria of natural-unnatural characteristics of the city, analyzes the spatial pattern characteristics of LST, and finally explores the impact of the indicators on the urban thermal environment by implementing a nonlinear regression through an RF model. The results provide decision support for urban planners and managers and provide a basis for subsequent research on the influence mechanism of the urban thermal environment.

The rest of the study is organized as follows. Section 2 explains the methodology used in the research framework, how the LST was retrieved and set to calculate the natural conditions/socioeconomic impact factors, and how the RF-based regression analysis model was constructed. Section 3 presents the experimental data and the analysis results. Section 4 discusses in detail the thermal environmental management measures and methods that can be explored for application given the results of this study, as well as the limitations of this study and possible directions for future improvement. Section 5 summarizes the conclusions of this study.

2. Methodology

The analysis process of this study consists of three main parts, as shown in Figure 1. The first part is the simulation of the urban thermal environment, which is characterized by using Landsat 8 image retrieval LST, where the images were acquired in summer on 28 August 2020. T the second part is the setting and measurement of the natural conditions/socioeconomic factors, which is based on the widely accepted neighborhood scale of OSM road network division and the measurement of the impact factors within each study unit. The third part is the construction of the RF-based impact factor assessment model, the optimization of its parameters, and evaluation of the results.

2.1. Study Area and Data

Located in east China and the central-western part of Shandong Province, Jinan is situated in the midlatitude zone, and due to the influence of solar radiation and geography, it belongs to the warm temperate continental monsoon climate zone with warm and rainy summers, making it one of the hottest cities in China in summer. Jinan has 10 municipal districts and 2 counties under its jurisdiction. The study area for this study is the central district of Jinan (Figure 1), with an area of 536 km^2 and a population of approximately 5.6 million. The high density of buildings and population in the area has influenced and shaped the hot climate and weather in the area, making it one of the cities with the most severe heat island effect in China (Figure 2).

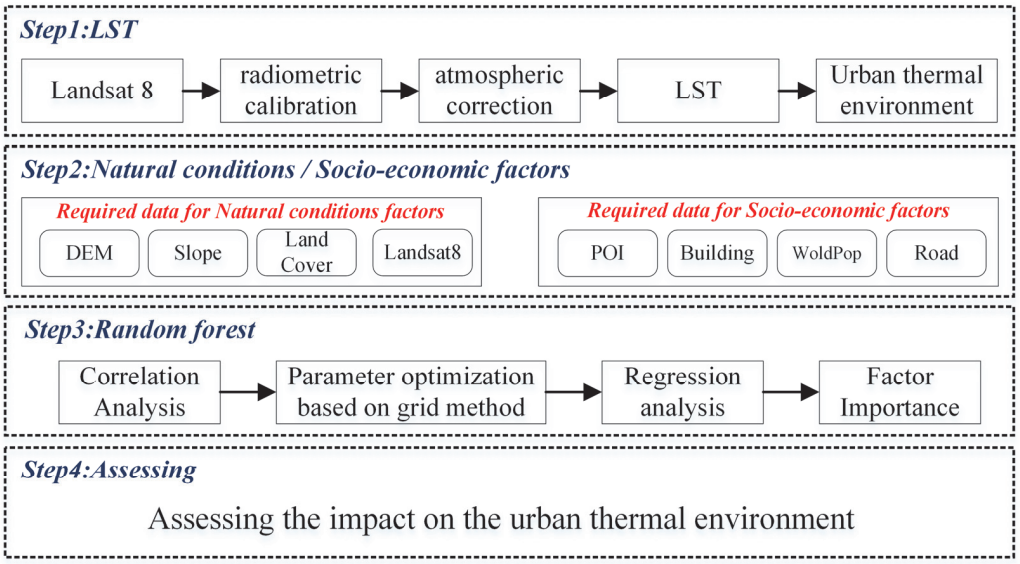

Figure 1. Research framework.

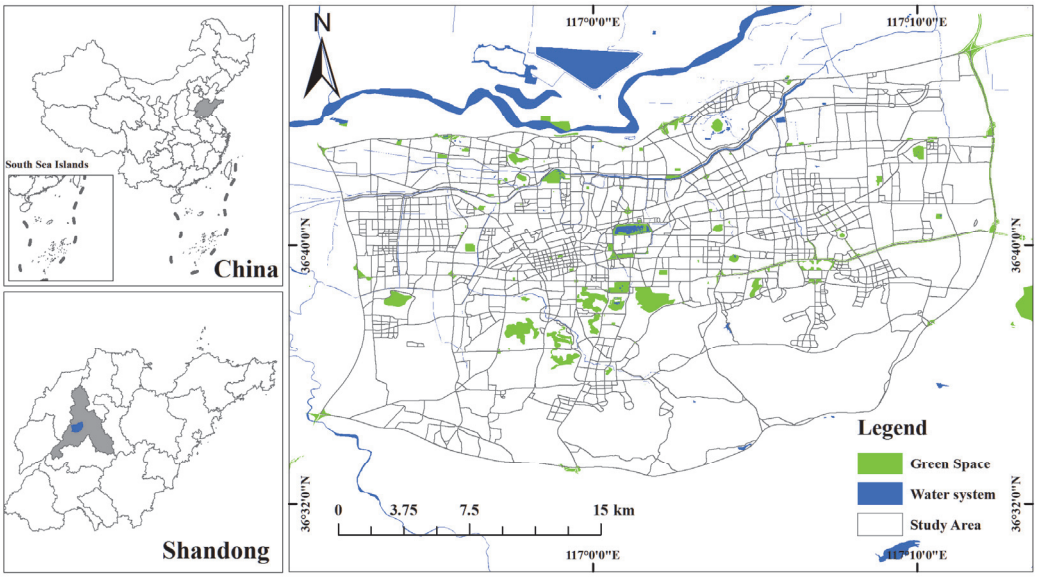

Figure 2. Study area and basic data.

The research data used in this study are shown in Table 1. The remote sensing image data, road network data, electronic map data, and POI data involved are all freely available online, and the spatial extent of the data covers the entire study area. Among them, 225,407 POI points and 5488 road data were collected in the study area. The POI and road network data were then preprocessed to remove duplicate points, sidewalks and invalid data records, and 1206 study units were delineated using the OSM road network.

2.2. Retrieval of Land Surface Temperature

The radiative transfer equation method uses the thermal infrared band data from satellites to achieve LST retrieval, and the calculation of the brightness value of the thermal radiation received by the satellite sensors is the radiative transfer equation. This method

retrieves the LST by estimating the atmospheric influence and deducting some of the errors. Its specific equation is as follows [36,37].

$$T_s = \frac{K_2}{\ln\left(\frac{K_1}{B(T_s)} + 1\right)}, \quad (1)$$

$$B(T_s) = \frac{\left[L_\lambda - L_\uparrow - \tau(1-\varepsilon)L_\downarrow\right]}{\tau\varepsilon} \quad (2)$$

where T_s is the true LST. In the Landsat-8 thermal infrared band, $K_1 = 774.885\ \mathrm{W{\cdot}m^{-2}{\cdot}sr^{-1}{\cdot}\mu m^{-1}}$ and $K_2 = 1321.079K$. $B(T_s)$ is the blackbody emissivity; ε is the surface specific emissivity; τ is the atmospheric transmittance in the thermal infrared band; L_λ is the image radiometric calibration; $L_\uparrow$ is the atmospheric upward radiometric intensity; $L_\downarrow$ is the atmospheric downward radiometric intensity; and K_1 and K_2 are coefficients. On the NASA website (https://atmcorr.gsfc.nasa.gov, accessed on 28 August 2020), the values of τ, $L_\uparrow$, and $L_\downarrow$ are 0.61, 3.24, and 4.97, respectively.

Table 1. Data List.

Data Name	Data Source	Acquisition Time	Data Type
Administrative Divisions	National Basic Geographic Database	/	Vector
Landsat8 image	http://www.gscloud.cn/	28 August 2020	Raster
Points of Interest	Gaode Map	September 2020	Vector
Land Cover Data	FROM-GLC10	2020	Raster
DEM	http://www.gscloud.cn/	2020	Raster
Building Data	Gaode Map	2020	Vector
Population data	WorldPop	2020	Raster
Road Data	OpenStreetMap	2020	Vector
Water System	OpenStreetMap	2020	Vector
Green Space	OpenStreetMap	2020	Vector

2.3. Assessment of Impact Factors Based on the RF Model

2.3.1. Measurement of Natural Conditions/Socioeconomic Factors

As the most dominant area where human activities alter the land surface, cities have developed typical urban characteristics with high density, height and intensity, which have a direct impact on urban climate. In this study, we chose two aspects, natural conditions/socioeconomic, to comprehensively measure urban characteristics. Their detailed factor descriptions and calculation formulae are shown in Table 2. Additionally, considering that the results of correlation analysis can show the positive and negative influencing factors and reveal the scientific accuracy and feasibility of factor selection, this study determines the directionality and intensity of each influencing factor by calculating the Pearson correlation between LST and different influencing factors.

Among them, the natural-conditions factor measures the native natural environment characteristics of the city by calculating the factors of elevation, NDVI, and distance to green space. Additionally, socioeconomic factors are mainly measured by building, road, and POI data, which can best represent the development intensity of the city. Specifically, the height and density of buildings and road density were calculated, and the primary classification of POI data was standardized based on the urban land classification system and definitions in the Urban Land Classification and Planning and Construction Land Standard issued by the Ministry of Housing and Urban—Rural Development of the People's Republic of China. On the basis of existing research, they were divided into seven categories—commercial, residential, industrial, public service, transportation, green space, and science and education—to measure their density to reflect the socioeconomic development intensity.

Table 2. The urban factors metrics considered in this study.

Types	Metrics	Formula and Description
Natural-condition indicators	DEM	/
	Slope	/
	NDVI	$NDVI = \frac{\rho NIR - \rho MIR}{\rho NIR + \rho MIR}$
	Distance to green space (DGS)	Proximity Analysis
	Distance to water system (DWS)	Proximity Analysis
Socioeconomic indicators	Average building height (BH)	$BH = \frac{\sum_{i=1}^{n} H_i}{n}$
	Building density (BD)	$BD = \frac{\sum_{i=1}^{n} (P_i \times H_i)}{S}$
	Road network density (RD)	$RD = \frac{\sum_{i=1}^{n} Roads_i}{Area}$
	Population (POP)	WorldPop data
	Road traffic POI density (RTPD)	Zoning Statistics
	Public Service POI Density (PSPD)	Zoning Statistics
	Residential POI Density (RPD)	Zoning Statistics
	Commercial POI Density (CPD)	Zoning Statistics
	Greenland Square POI Density (GPD)	Zoning Statistics
	Science and education POI density (SEPD)	
	Industrial POI Density (IPD)	Zoning Statistics

2.3.2. Factor Assessment Based on the Random Forest Model

In urban studies, the RF algorithm has been validated as a suitable regression analysis method [38], and is a highly flexible and comprehensive learning algorithm that trains models by integrating the results of all randomly generated classification and regression decision trees more accurately than traditional regression methods. In this study, natural conditions/socioeconomic factors are used as independent variables, and LST is put into the RF regression model as a dependent variable for the fitting operation, where approximately two-thirds of the data are used to construct the RF regression model and the remaining third is used for accuracy validation. Among them, the selection of parameters is determined by the grid search method, and the range of parameter sets determines the time of grid search calculation [39]; the larger the range is, the longer the calculation time. The study determined the screening range of the number of decision trees (0–100) by the dichotomous method, and the ranges of the maximum number of features and the maximum depth of the tree were determined with reference to the sample conditions. Finally, a reasonable and scientific regression fitting model for LST influencing factors is constructed by tenfold cross-validation.

The modeling programming language of this study is Python version 3.6, and the core algorithm comes from the open-source machine learning library scikit-learn. The accuracy validation of the model uses R^2 and mean square error (MSE) [40], which is the ratio of the square root of the sum of the squared deviations of the observed and true values to the number of observations, to measure the deviation of the observed values from the true values and reflect the actual situation of the prediction error.

3. Results

3.1. Land Surface Temperature Retrieval and SUHI Area Identification Results

Figure 3 shows the spatial and temporal distribution of LST in Jinan. Spatially, there is a synergistic phenomenon between the thermal environment and the spatial pattern of natural conditions/socioeconomics in the study area. Smaller areas of speckled heat island regions are also presented in addition to the urban center. The high-temperature areas are

further enhanced, except for some squares, parks, and well-greened neighborhoods. Most of them develop into high-temperature areas, including a large number of construction sites, commercial areas, densely populated stations, and industrial enterprise areas as high-temperature areas. The high-temperature areas cover almost the whole study area, and the thermal environment is generally poor. From the LST results, the average LST is 28.55 °C. The maximum value of LST is 42.29 °C, which is located in the inner city, and the minimum value is 14.22 °C, which is located on the surface of the water body. The high values are concentrated in the eastern part of the study area, mainly in the built-up areas. The spatial pattern is mainly driven by the town cohesion axis, showing a "point-line surface" urban thermal environment. The abnormally high-temperature zones within the city are mainly concentrated in the urban center, industrial areas with high energy consumption, stations, and bare land, and the strong heat island zones (most of the Lixia district, the northern part of the city central district, the eastern part of the Huaiyin district and the southern part of the Tianqiao district) are connected to the surrounding areas through the main urban roads. Specifically, the low-temperature area is mainly distributed in the study area of scenic spots, parks, large lakes, springs, rivers, mountains, and other vegetation and water bodies near the densely distributed areas of the blocks, such as the Dragon Cave scenic area and the Golden Valley Landscape Gallery scenic area in the south, the Thousand Buddha Mountain scenic area, Huashan Lake Park, Jinan Zoo and Baotu in the north. High-temperature areas are mainly distributed in the rapidly developing and building factory-intensive eastern industrial areas.

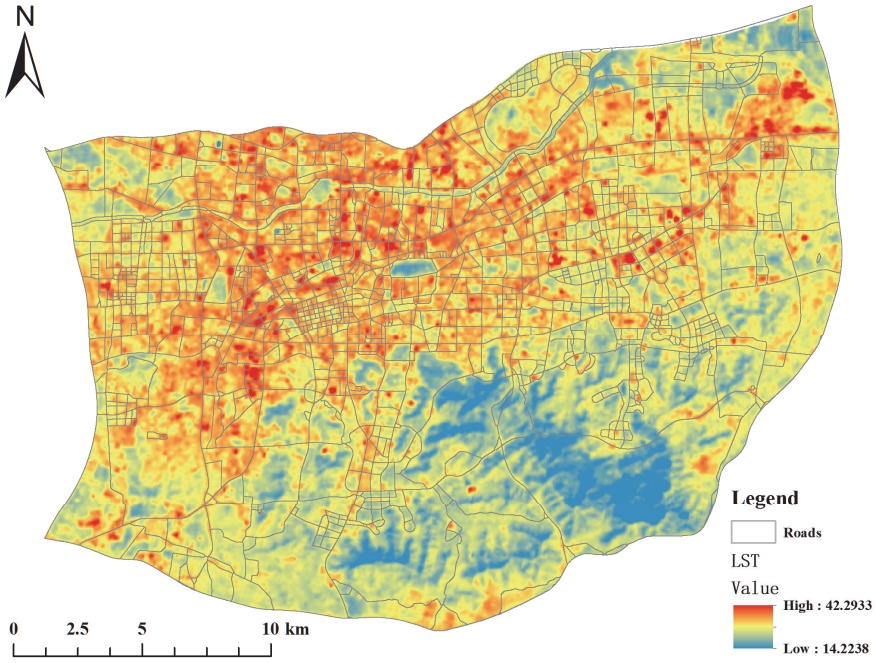

Figure 3. Land surface temperature retrieval results.

3.2. Results of Natural Condition/Socioeconomic Indicator Measurements

In this study, Pearson correlation analysis was used to verify the relationship between LST and natural conditions/socioeconomic factors, as shown in Figure 4 Most of the influencing factors showed significant correlations (two-sided) with LST at the level of 0.001. Among them, the strongest correlation is NDVI (−0.61), and the lowest is SLOPE (0.12). Specifically, natural factors such as DEM, NDVI, DGS, and DWS all show significant negative correlations with LST, i.e., the higher the elevation, the lusher the vegetation, etc., the lower the LST. This indicates that this influencing factor can significantly mitigate the urban heat island effect. The meteorological conditions provided by the areas with high

DEM values and the shadows of the mountains reduce the LST; however, the natural surface represented by green areas and water bodies can release heat through the evaporation of water. In addition, the transpiration of vegetation foliage also effectively reduces the LST. In contrast, the influencing factors represented by buildings (BH, BD), roads (RD), and POI density have a positive relationship with LST. The higher the buildings and roads are, the denser the population distribution, and the higher the LST. The impervious surface has a significant enhancement effect on the LST, which is because various hard pavements are mainly composed of cement, asphalt, concrete, etc. These materials have a strong ability to absorb solar radiation, and at the same time, there are many buildings in the urban area, the air circulation is complicated, and there is more artificial heat release, which makes it difficult to dissipate heat and the LST is higher.

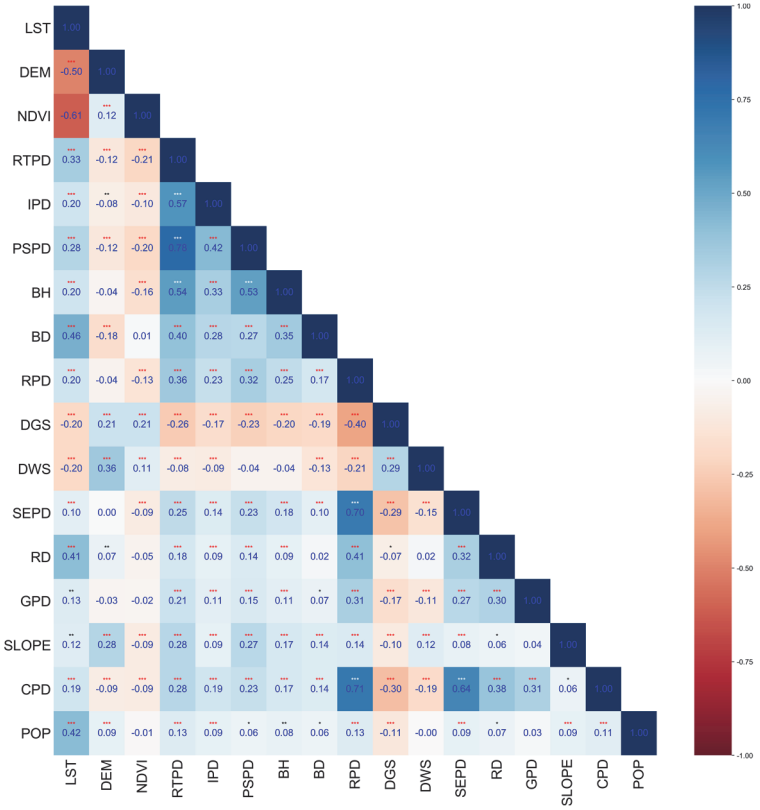

Figure 4. Correlation analysis results. "*", "**", and "***" are the results of significance tests, which indicate that the correlation coefficients are significant at the 0.05, 0.01, and 0.001 levels, respectively.

The results of natural conditions/socioeconomic factor measurements are shown in Figure 5. Overall, DEM, SLOPE, and NDVI show almost the same spatial trend and generally show a distribution pattern of high in the south–low in the north, and their high- and low-value areas have similarities, with high values mainly concentrated near mountainous areas with less human activities, such as the southern mountainous areas, and low-value areas mainly concentrated in some areas with dense buildings. Water bodies DGS and DWS also show the same spatial consistency, with most of the high-value areas located in the peripheral boundary areas of the study area and a wide range of low-value areas within the urban center. The high-value areas are mainly concentrated in urban areas with high human activities, industrial and mining land, urban road land, etc., and are concentrated in blocks in the northern area, while they are scattered in other areas. The spatial patterns of RD and POP are similar, which confirms that the distribution of roads, as a necessary condition for urban travel, is often related to the distribution of the population. The spatial distribution of GPD is the most fragmented, and the small regional centers are

clustered. The most prominent, similar to the distribution of green parks in Jinan, have the greatest spatial heterogeneity. IPD shows a combined structure of central gathering, eastern main roads, and station gathering and a spatial trend of expanding radially along the main roads to the east centered on the earlier developed industries around the central part of the study area.

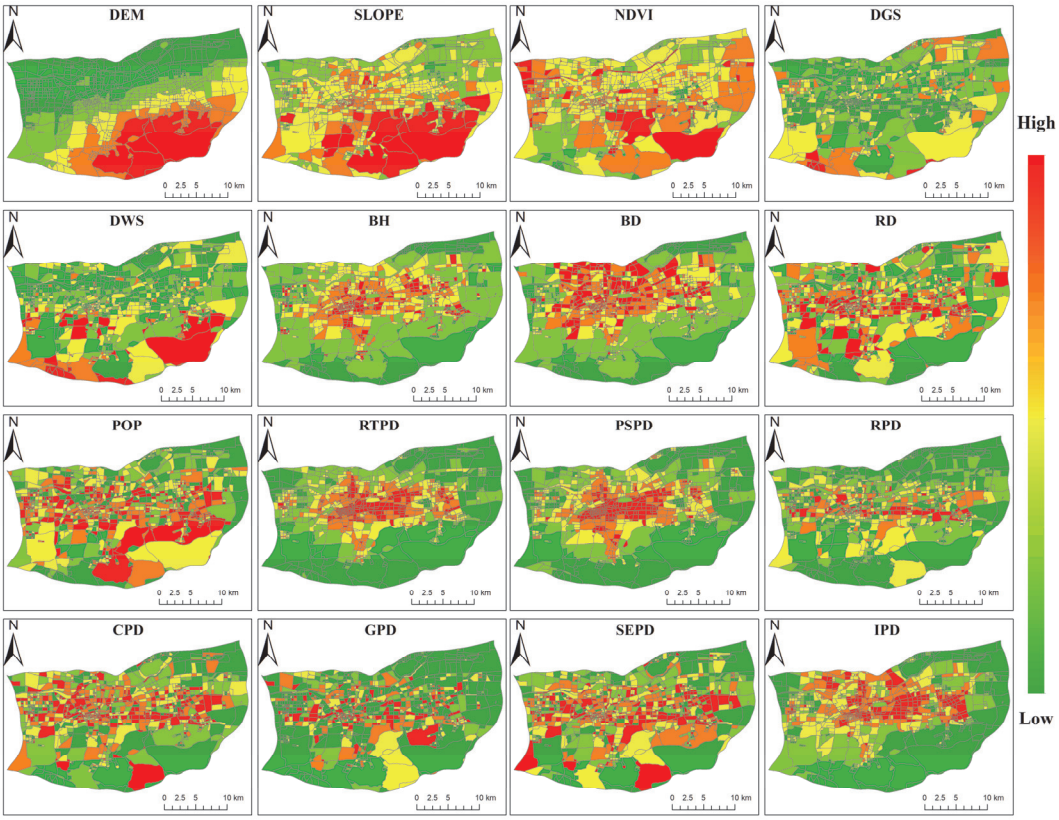

Figure 5. Measurement results of natural conditions/socioeconomic factors.

3.3. Assessing the Impact of Indicators on Urban Heat Islands

3.3.1. Grid Search Method for Determining Hyperparameters

The tuning of RF model parameters is crucial to improve the recognition accuracy. To establish a better RF regression model, this study uses the grid search method to tune the parameters. The natural condition factor, socioeconomic factor and all factors are input into the regression model, and the maximum number of features and the maximum depth of the tree are set to 5 and 4, respectively, considering the sample size and the number of features. On this basis, the number of decision trees greatly affects the fitting accuracy of the regression model; therefore, the comparison results of the number of decision trees applying the grid search method to tune the parameters are shown in Figure 6. To determine the best recognition accuracy, the number of trees in the RF was set to 1–100 trees. Model accuracy and MSE results were analyzed for each group of 100 control experiments. The average accuracy of the natural condition factor regression model reached 0.42, the average MSE was 0.18, and the highest recognition accuracy reached 0.49 when the number of trees was 47, and the value of MSE was 1.4; the average accuracy of the socioeconomic regression model reached 0.54, and the highest recognition accuracy reached 0.56 when the number of trees was 78, and the value of MSE was 1.32; inputting all factors into the regression model, the average accuracy reached 0.82, and the highest identification accuracy reached 0.86 when the number of trees was 14, which is higher than the fitting accuracy of the single-aspect factor regression model. Additionally, the value of MSE was only 0.8, which

is the best model to meet the requirements. The high-intensity effect of natural condition factors on the urban thermal environment was demonstrated.

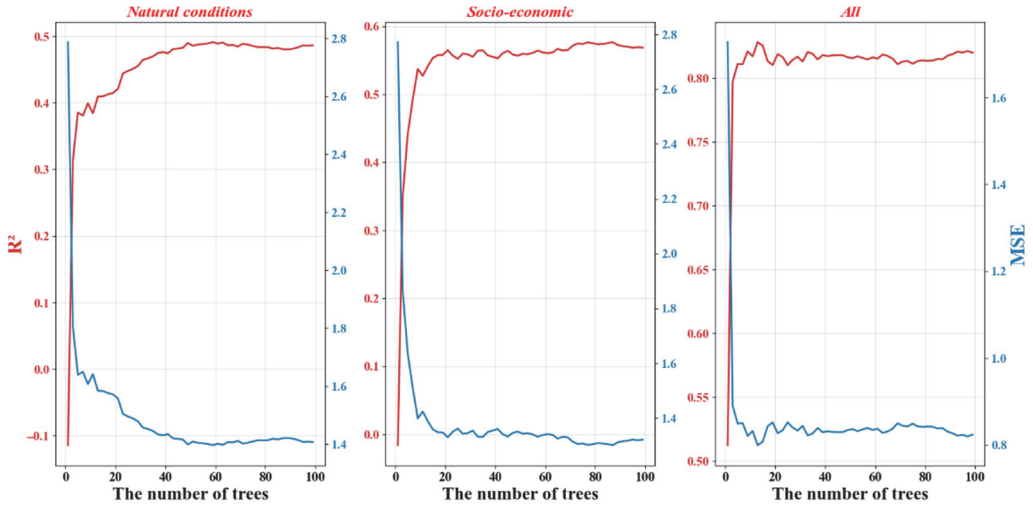

Figure 6. Experimental results comparing regression accuracy and MSE. where the red line represents the regression accuracy and the blue line represents the MSE.

3.3.2. Assessing the Importance of Natural and Socioeconomic Factors

The RF model can quantitatively assess the magnitude of the influence of each influencing factor on the spatial variation in LST in the study area. According to the results of the contribution of each factor of the RF model (Figure 7), it was found that the importance of different factors on LST was both synergistic and heterogeneous across models. Overall, the natural conditions model (Model A) was dominated by BD, the socioeconomic model (Model B) was dominated by DEM, and the natural conditions/socioeconomic model (Model C) was dominated by BD. In Model A, the influencing factors on LST are, in descending order, BDI, PD, RD, PSPD, BH, POP, RPD, CPD, SEPD, and GSPD; in Model B, the influencing factors on LST are, in descending order, DEM, NDVI, SLOPE, DGS, and DWS; in Model C, the influencing factors on LST are higher for BD, DEM, RTPD, NDVI, IPD, SLOPE, and BH, and the rest of the factors are to a lesser extent for LST. Based on the results of the above analysis, urban building land, land use, and vegetation are the dominant factors leading to the spatial differentiation of LST in the study area. The influence of BD is greater than 0.3 in both Models A and C, indicating that building is an important factor leading to the spatial differentiation of LST. The influence of elevation and slope adds up to more than 0.2 in Model C and even more than 0.45 in Model B, indicating that elevation and slope are all types of POI densities that play a role in LST to a lesser extent, but the sum of importance exceeds 0.5 overall, indicating that a single human socioeconomic activity has a small influence on the spatial variation of LST in the study area but has a greater global correlation with LST. Therefore, socioeconomic activities are important potential influences on the urban thermal environment. As a whole, the spatial differentiation of LST in the main urban area of Jinan is the result of the combined effect of natural conditions and socioeconomics, with DEM and vegetation cover among natural factors having larger contributions and building sites, roads, and POI among socioeconomics all having larger contributions.

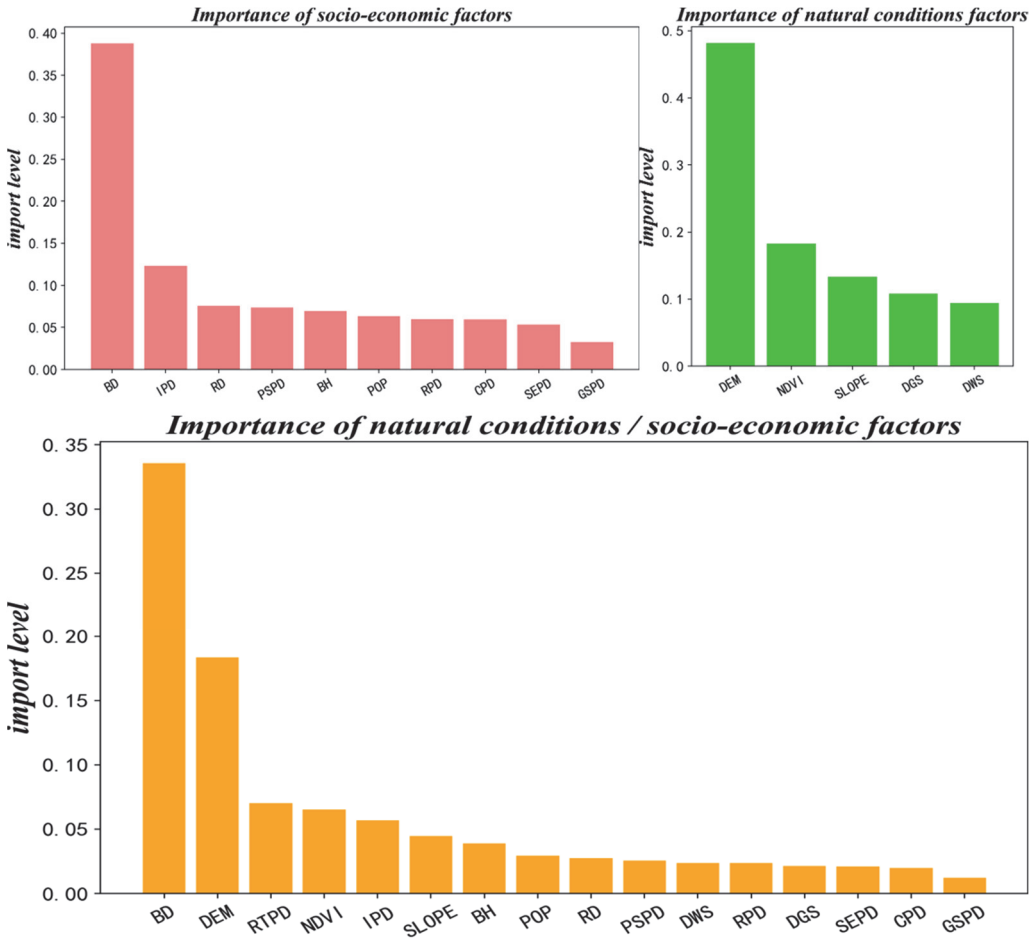

Figure 7. The results of the contribution of each factor of the RF model.

4. Discussion

4.1. Implications for Urban Planning to Mitigate the Heat Island Effect

Previous analyses of the causes of urban heat island enhancement have been attributed to industrialization development, population migration and atmospheric effects [41,42], but little attention has been given to the comprehensive analysis of natural conditions/socioeconomic factors [43]. The intensity of the heat island effect is the result of the interaction and mutual coupling of socioeconomic and natural conditions; therefore, in this study, impact factor analysis is conducted based on big data to measure the natural conditions and socioeconomic multiple characteristics, which can better reflect the driving factors of the regional thermal environment. Urbanization has led to the conversion of large areas of natural surfaces into artificial impervious surfaces [44], urban buildings and urban water bodies have a direct impact on the urban microclimate, and building materials such as masonry and concrete have a lower albedo than green spaces, reducing evaporation and soil moisture [45]; thus, these factors are also important for the thermal environment of hot cities and need to be explored in future studies. In the study of the factors influencing urban heat islands, it was found that the central city of Jinan is high in the south and low in the north, the northern and eastern areas are convenient for infrastructure construction and industrial and urban land expansion, and land use is easily shifted from vegetation to industrial land, thus promoting the deterioration of the urban thermal environment [46]. Second, various areas with high POI densities, represented by commercial and industrial areas, have a certain contribution to urban heat islands. In the north of the study area, spring lakes and green parks in the south of the Yellow River are widely distributed, with high soil water content, located in the plains, with higher temperature and higher

evapotranspiration; in the east of the study area, with convenient transportation, a large number of population inflows in the central city, rapid industrial development, and high aerosol emissions, increasing the inverse radiation of the atmosphere, especially in summer, contribute more to the urban heat island [47]. Compared to the southern part of the study area, the vegetation cover is higher compared to other areas, and the thermal environment is in good condition [48].

Combining the abovementioned thermal environments in different regions, the contributions of different influencing factors are analyzed to design effective thermal environment optimization measures [49]. According to the natural conditions and socioeconomic development characteristics of the cities in the study area, it is concluded that controlling the scale and layout of buildings, controlling the scale of the urban population, increasing the urban greening rate (especially road greening), and strengthening greening construction in the heat island center area can effectively mitigate the urban heat island effect, which can provide a reference for urban planning and construction [50]. (1) A reasonable urban planning scheme should be established to encourage medium- and high-density land development at the level of urban construction activities. The construction of urban roads and some other heat source structures can be reduced to reduce the energy consumed by public infrastructure after operation [51]; however, the transformation of arable land, forests and water bodies around the eastern industrial agglomeration into construction land should be reduced to curb the further deterioration of the heat island in the industrial area; (2) According to the spatial distribution of LST in Hohhot city, it can be seen that the areas with obvious urban heat island effects are also the areas where there are flows of people is densely populated areas, such as the railway station and Quancheng Square. The corresponding building density is higher in densely populated areas, which consumes considerable energy and generates considerable artificial heat. Therefore, relevant policies should be formulated to limit the quantity of the urban population and improve the quality of the population, and sustainable urban planning should be carried out to control the scale of the urban population and building density [52]. (3) Urban green space is an important factor in regulating the urban ecological climate and coordinating climate change. Especially considering the mutual influence of RD as well as NDVI and other indicators, the planning and design of urban road traffic systems should fully consider the ventilation of the city, and green evaporation on both sides of the road can optimize the urban thermal environment in summer. Smaller strips of green space can also connect multiple scattered green spaces to form a unified ecological corridor. In practice, the vertical level of road green space plants should be enriched, and the variety of trees and shrubs should be increased [53].

4.2. Limitations and Future Avenues

Based on the results of this study, we can plan some urban natural–unnatural factors within the index guidance to ensure a smaller building area ratio, higher vegetation coverage, lower building density and appropriate point density of POI types with a better cooling effect on LST. The results of this study help to deepen the understanding of the relationship between natural urban conditions as well as socioeconomic characteristics and the urban thermal environment and aim to provide practical suggestions on how to improve the urban thermal environment through rational planning and management.

This study focuses on the impact of the thermal environment in Jinan city during the daytime in summer, focusing on the time of maximum heat island intensity, but the analysis is not comprehensive enough to explore the changes in months and seasons. Another limitation of this study was that it was limited by the lack of dynamic data, the application of spatial big data is greater, but the supplement of temporal big data is missing, and the factor measurement standard needs to be improved. This limitation provides an idea for future research to accurately examine the effects of time and data sources [54].

5. Conclusions

Based on big data, this study analyzes the dominant influencing factors of the urban thermal environment under the dual perspective of natural conditions/socioeconomic factors by retrieving the LST of the central city area of Jinan and elucidates the relationship between the urban thermal environment and natural-unnatural influencing elements. On this basis, specific measures to mitigate the urban heat island effect are explored in depth. The analytical ideas and results are transferable and instructive. The study found the following.

(1) From the whole study area, the urban thermal environment was poor, the urban high-value LST area was large and agglomerative, the abnormally high-temperature area is mainly concentrated in the urban center, industrial areas with high energy consumption, stations, and bare land, and the urban heat island mainly expands outward from the urban center along the traffic route.

(2) All influencing factors were significantly correlated with LST, among which the strongest correlation was NDVI (−0.61) and the lowest was SLOPE (0.12). DEM, NDVI, DGS, and DWS were negatively correlated with LST, while all other factors are positively correlated.

(3) The fitted R^2 of single regression models were all below 0.5, and the fitted R^2 reached 0.86 when natural conditions/socioeconomic factors were included in the regression models. All regression results show significant differences, with BD contributing the most to the regional thermal environment, followed by DEM, NDVI, RTPD, etc. The contribution of thermal effects of single POI types is small, but the combined contribution exceeds 0.5.

(4) Building scale and layout, urban population scale, urban greening rate (especially road greening), etc., are improvement directions that can effectively mitigate the urban heat island effect.

Author Contributions: X.L., writing—original draft preparation and methodology; H.W. and H.C., writing—review and editing; X.L., S.G. and H.C., methodology and resources. All authors have read and agreed to the published version of the manuscript.

Funding: The APC was funded by Shandong Engineering Research Center for Environmental Protection and Remediation on Groundwater.

Institutional Review Board Statement: Not applicable.

Informed Consent Statement: Not applicable.

Data Availability Statement: Data sources can be found in the data presentation Section 2.1.

Conflicts of Interest: The authors declare that they have no known competing financial interests or personal relationships that could have appeared to influence the work reported in this paper.

References

1. Imhoff, M.L.; Zhang, P.; Wolfe, E.R.; Bounoua, L. Remote sensing of the urban heat island effect across biomes in the continental USA. *Remote Sens. Environ.* **2010**, *114*, 504–513. [CrossRef]
2. Chen, M.; Liu, W.; Lu, D. Challenges and the way forward in China's new-type urbanization. *Land Use Policy* **2016**, *55*, 334–339. [CrossRef]
3. Fan, X.; Duan, Q.; Shen, C.; Wu, Y.; Xing, C. Global surface air temperatures in CMIP6: Historical performance and future changes. *Environ. Res. Lett.* **2020**, *15*, 104056. [CrossRef]
4. Wu, Z.; Ren, Y. A bibliometric review of past trends and future prospects in urban heat island research from 1990 to 2017. *Environ. Rev.* **2019**, *27*, 241–251.
5. Liu, K.; Li, X.; Wang, S.; Li, Y. Investigating the impacts of driving factors on urban heat islands in southern China from 2003 to 2015. *J. Clean. Prod.* **2020**, *254*, 120141. [CrossRef]
6. Alcoforado, M.J.; Andrade, H. Global warming and the urban heat island. In *Urban Ecology*; Springer: Berlin, Germany, 2008; pp. 249–262.
7. Yang, J.; Wang, Z.-H.; Kaloush, K.E. Environmental impacts of reflective materials: Is high albedo a 'silver bullet' for mitigating urban heat island? *Renew. Sustain. Energy Rev.* **2015**, *47*, 830–843. [CrossRef]

8. Gago, E.J.; Roldan, J.; Pacheco-Torres, R.; Ordóñez, J. The city and urban heat islands: A review of strategies to mitigate adverse effects. *Renew. Sustain. Energy Rev.* **2013**, *25*, 749–758. [CrossRef]
9. Lai, D.; Liu, W.; Gan, T.; Liu, K.; Chen, Q. A review of mitigating strategies to improve the thermal environment and thermal comfort in urban outdoor spaces. *Sci. Total Environ.* **2019**, *661*, 337–353. [CrossRef]
10. Li, Z.L.; Tang, B.H.; Wu, H.; Ren, H.; Yan, G.; Wan, Z.; Trigo, L.F.; Sobrino, J.A. Satellite-derived land surface temperature: Current status and perspectives. *Remote Sens. Environ.* **2013**, *131*, 14–37. [CrossRef]
11. Liu, Y.; Hiyama, T.; Yamaguchi, Y. Scaling of land surface temperature using satellite data: A case examination on ASTER and MODIS products over a heterogeneous terrain area. *Remote Sens. Environ.* **2006**, *105*, 115–128. [CrossRef]
12. Sattari, F.; Hashim, M. A brief review of land surface temperature retrieval methods from thermal satellite sensors Middle-East. *J. Sci. Res.* **2014**, *22*, 757–768.
13. Zhao, Y.; Wu, Q.; Wei, P.; Zhao, H.; Zhang, X.; Pang, C. Explore the Mitigation Mechanism of Urban Thermal Environment by Integrating Geographic Detector and Standard Deviation Ellipse (SDE). *Remote Sens.* **2022**, *14*, 3411. [CrossRef]
14. Ma, L.; Yang, Z.; Zhou, L.; Lu, H.; Yin, G. Local climate zones mapping using object-based image analysis and validation of its effectiveness through urban surface temperature analysis in China. *Build. Environ.* **2021**, *206*, 108348. [CrossRef]
15. Watkins, R.; Palmer, J.; Kolokotroni, M. Increased temperature and intensification of the urban heat island: Implications for human comfort and urban design. *Built Environ.* **2007**, *33*, 85–96. [CrossRef]
16. Webb, B. The use of urban climatology in local climate change strategies: A comparative perspective. *Int. Plan. Stud.* **2017**, *22*, 68–84. [CrossRef]
17. Hokao, K.; Phonekeo, V.; Srivanit, M. Assessing the impact of urbanization on urban thermal environment: A case study of Bangkok Metropolitan. *Int. J. Appl.* **2012**, *2*, 7.
18. Chen, S.; Hu, D. Parameterizing anthropogenic heat flux with an energy-consumption inventory and multi-source remote sensing data. *Remote Sens.* **2017**, *9*, 1165. [CrossRef]
19. Wollmann, C.A.; Hoppe, I.L.; Gobo, J.P.A.; Simioni, J.P.D.; Costa, I.T.; Baratto, J.; Shooshtarian, S. Thermo-hygrometric variability on waterfronts in negative radiation balance: A case study of balneário Camboriú/SC, Brazil. *Atmosphere* **2021**, *12*, 1453. [CrossRef]
20. Giorgio, G.A.; Ragosta, M.; Telesca, V. Climate variability and industrial-suburban heat environment in a Mediterranean area. *Sustainability* **2017**, *9*, 775. [CrossRef]
21. Wang, R.; Min, J.; Li, Y.; Hu, Y.; Yang, S. Analysis on Seasonal Variation and Influencing Mechanism of Land Surface Thermal Environment: A Case Study of Chongqing. *Remote Sens.* **2022**, *14*, 9. [CrossRef]
22. Zhang, N.; Ye, H.; Wang, M.; Li, Z.; Li, S.; Li, Y. Response relationship between the regional thermal environment and urban forms during rapid urbanization (2000–2010–2020): A case study of three urban agglomerations in China. *Remote Sens* **2022**, *14*, 3749. [CrossRef]
23. Guerri, G.; Crisci, A.; Cresci, I.; Congedo, L.; Munafò, M.; Morabito, M. Residential Buildings' Real Estate Values Linked to Summer Surface Thermal Anomaly Patterns and Urban Features: A Florence (Italy) Case Study. *Sustainability* **2022**, *14*, 8412. [CrossRef]
24. Kim, Y.-H.; Baik, J.-J. Daily maximum urban heat island intensity in large cities of Korea. *Theor. Appl. Climatol.* **2004**, *79*, 151–164. [CrossRef]
25. Halder, B.; Bandyopadhyay, J.; Banik, P. Evaluation of the climate change impact on urban heat island based on land surface temperature and geospatial indicators. *Int. J. Environ. Res.* **2021**, *15*, 819–835. [CrossRef]
26. Peng, X.; Wu, W.; Zheng, Y.; Sun, J.; Hu, T.; Wang, P. Correlation analysis of land surface temperature and topographic elements in Hangzhou, China. *Sci. Rep.* **2020**, *10*, 10451. [CrossRef] [PubMed]
27. Chun, B.; Guldmann, J.-M. Two- and Three-Dimensional Urban Core Determinants of the Urban Heat Island: A Statistical Approach. *J. Environ. Sci. Eng. B* **2012**, *1*, 363–378.
28. Neis, P.; Zielstra, D. Recent developments and future trends in volunteered geographic information research: The case of OpenStreetMap. *Future Int.* **2014**, *6*, 76–106. [CrossRef]
29. Graham, M.; Shelton, T. Geography and the future of big data, big data and the future of geography. *Dialogues Hum. Geogr.* **2013**, *3*, 255–261. [CrossRef]
30. Chen, K.; Lu, W.; Xue, F.; Tang, P.; Li, L.H. Automatic building information model reconstruction in high-density urban areas: Augmenting multi-source data with architectural knowledge. *Autom. Constr.* **2018**, *93*, 22–34. [CrossRef]
31. Liu, X.; Chen, M.; Claramunt, C.; Batty, M.; Kwan, M.P.; Senousi, A.M.; Cheng, T.; Strobl, J.; Cöltekin, A.; Wilson, J.; et al. Geographic information science in the era of geospatial big data: A cyberspace perspective. *Innovation* **2022**, *3*, 100279. [CrossRef]
32. Zhao, P.; Liu, X.; Shen, J.; Chen, M. A network distance and graph-partitioning-based clustering method for improving the accuracy of urban hotspot detection. *Geocarto Int.* **2019**, *34*, 293–315. [CrossRef]
33. He, X.; Cao, Y.; Zhou, C. Evaluation of polycentric spatial structure in the urban agglomeration of the pearl river delta (PRD) based on multi-source big data fusion. *Remote Sens.* **2021**, *13*, 3639. [CrossRef]
34. Yin, J.; Dong, J.; Hamm, N.A.; Li, Z.; Wang, J.; Xing, H.; Fu, P. Integrating remote sensing and geospatial big data for urban land use mapping: A review. *Int. J. Appl. Earth Obs. Geoinf.* **2021**, *103*, 102514. [CrossRef]
35. Tran, D.X.; Pla, F.; Latorre-Carmona, P.; Myint, S.W.; Caetano, M.; Kieu, H.V. Characterizing the relationship between land use land cover change and land surface temperature. *ISPRS J. Photogramm. Remote Sens.* **2017**, *124*, 119–132. [CrossRef]

36. Yu, X.; Guo, X.; Wu, Z. Land surface temperature retrieval from Landsat 8 TIRS—Comparison between radiative transfer equation-based method, split window algorithm and single channel method. *Remote Sens.* **2014**, *6*, 9829–9852. [CrossRef]
37. Zhou, S.; Cheng, J. An improved temperature and emissivity separation algorithm for the advanced Himawari imager. *IEEE Trans. Geosci. Remote Sens.* **2020**, *58*, 7105–7124. [CrossRef]
38. Li, K.; Chen, Y.; Li, Y. The random forest-based method of fine-resolution population spatialization by using the international space station nighttime photography and social sensing data. *Remote Sens.* **2018**, *10*, 1650. [CrossRef]
39. Buttan, Y.; Chaudhary, A.; Saxena, K. An improved model for breast cancer classification using random forest with grid search method. Proceedings of Second International Conference on Smart Energy and Communication; Springer: Singapore, 2021; pp. 407–415.
40. Pekel, E. Estimation of soil moisture using decision tree regression. *Theor. Appl. Climatol.* **2020**, *139*, 1111–1119. [CrossRef]
41. Zhang, H.; Qi, Z.F.; Ye, X.Y.; Cai, Y.B.; Ma, W.C.; Chen, M.N. Analysis of land use/land cover change, population shift, and their effects on spatiotemporal patterns of urban heat islands in metropolitan Shanghai, China. *Appl. Geogr.* **2013**, *44*, 121–133. [CrossRef]
42. Lawrence, M.G.; Lelieveld, J. Atmospheric pollutant outflow from southern Asia: A review. *Atmos. Chem. Phys.* **2010**, *10*, 11017–11096. [CrossRef]
43. Zhu, S.; Liu, Y.; Hua, J.; Zhang, G.; Zhou, Y.; Xialng, J. Monitoring spatio-temporal variance of an extreme heat event using multiple-source remote sensing data. *Chin. Geogr. Sci.* **2018**, *28*, 744–757. [CrossRef]
44. Sadiq Khan, M.; Ullah, S.; Sun, T.; Rehman, A.U.; Chen, L. Land-use/land-cover changes and its contribution to urban heat Island: A case study of Islamabad, Pakistan. *Sustainability* **2020**, *12*, 3861. [CrossRef]
45. Chatzidimitriou, A.; Yannas, S. Microclimate development in open urban spaces: The influence of form and materials. *Energy Build.* **2015**, *108*, 156–174. [CrossRef]
46. Singh, P.; Kikon, N.; Verma, P. Impact of land use change and urbanization on urban heat island in Lucknow city, Central India. A remote sensing based estimate. *Sustain. Cities Soci.* **2017**, *32*, 100–114. [CrossRef]
47. Chen, X.; Zhang, Y. Impacts of urban surface characteristics on spatiotemporal pattern of land surface temperature in Kunming of China. *Sustain. Cities Soci.* **2017**, *32*, 87–99. [CrossRef]
48. Wu, Z.; Man, W.; Ren, Y. Influence of tree coverage and micro-topography on the thermal environment within and beyond a green space. *Agric. For. Meteorol.* **2022**, *316*, 108846. [CrossRef]
49. Wang, G.Q.; Zheng, B.H.; Yu, H.; Peng, X. Green space layout optimization based on microclimate environment features. *Int. J. Sustain. Dev. Plan.* **2019**, *14*, 9–19. [CrossRef]
50. Feng, X.; Xiu, C.; Bai, L.; Zhong, Y.; Wei, Y. Comprehensive evaluation of urban resilience based on the perspective of landscape pattern: A case study of Shenyang city. *Cities* **2020**, *104*, 102722. [CrossRef]
51. Nichols, B.G.; Kockelman, K.M. Life-cycle energy implications of different residential settings: Recognizing buildings, travel, and public infrastructure. *Energy Policy* **2014**, *68*, 232–242. [CrossRef]
52. Omer, A.M. Energy, environment and sustainable development. *Renew. Sustain. Energy Rev.* **2008**, *12*, 2265–2300. [CrossRef]
53. Li, B.; Xing, H.; Cao, D.; Yang, G.; Zhang, H. Exploring the Effects of Roadside Vegetation on the Urban Thermal Environment Using Street View Images. *Int. J. Environ. Res. Public Health* **2022**, *19*, 1272. [CrossRef] [PubMed]
54. Zhou, D.; Xiao, J.; Bonafoni, S.; Berger, C.; Deilami, K.; Zhou, Y.; Frolking, S.; Yao, R.; Qiao, Z.; Sobrino, J.A. Satellite remote sensing of surface urban heat islands: Progress, challenges, and perspectives. *Remote Sens.* **2018**, *11*, 48. [CrossRef]